Journal of Power Sources xxx (xxxx) 229854

Contents lists available at ScienceDirect

Journal of Power Sources

journal homepage: www.elsevier.com/locate/jpowsour

Coating internal surface of porous electrode for decreasing the ohmic resistance and shifting oxygen reduction reaction pathways in solid oxide fuel cells

Yun Chen [a], Sergio A. Paredes-Navia [a], Cesar-Octavio Romo-De-La-Cruz [a], Liang Liang [a], Andre Fernandes [a], Alec Hinerman [a], Jacky Prucz [a], Mark Williams [b], Xueyan Song [a,*]

[a] Department of Mechanical & Aerospace Engineering, West Virginia University, Morgantown, WV, 26506, USA
[b] Mark Williams – Keylogic Corporate, 3168 Collins Ferry Road Morgantown, West Virginia, 26505, USA

ARTICLE INFO

Keywords:
Solid oxide fuel cell
Atomic layer deposition
Cobalt oxide
Platinum
Oxygen reduction reaction

ABSTRACT

For mixed conductor $La_{0.6}Sr_{0.4}Co_{0.2}Fe_{0.8}O_{3-x}$ (LSCF) in solid oxide fuel cells (SOFCs), cation surface segregation such as volatile Sr and consequently losing conductivity and active sites for the oxygen reduction reaction (ORR) are problematic. To mitigate the cation segregation, a practical approach is to apply a conformal surface coating. Nevertheless, the coating layer would inevitably alter the ORR pathways that initially take place on the backbone surface. In this study, the unary electrocatalyst of Pt or CoO_x was applied to the LSCF/Sm-doped CeO_2 (SDC) composite electrode of inherently functional SOFCs. Both ALD coating layers evolve strong interaction with the composite cathode. Upon operations, the Pt coating layer remains conformal on LSCF grain surfaces but turns into discrete particles on SDC. For the CoO_x coating, the conformal layer grows to be the discrete nano-grains on both the LSCF and SDC grains. ALD coating of the cathode alone reduces the cell ohmic resistance. The ALD-induced conductivity change is ascribed to different mechanisms. This study presents a novel and feasible approach to apply a conformal, dense coating layer on the surface of a mixed conductor, simultaneously increasing the conductivity and durability of the SOFC cathode.

1. Introduction

In comparison with the solar, wind, and tidal power that is site-specific and intermittent, solid oxide fuel cells (SOFCs) offer unrivaled high efficiency and excellent fuel flexibility. However, current SOFC technology is still hindered by high production costs and insufficient durability. For utility-scale stationary power systems, the SOFCs are expected to have durability towards 40,000 h (5 years) continuous operation. The low conductivity and the sluggish electrode kinetics in SOFC cathodes are still causing significant ohmic and polarization losses over the prolonged operation at elevated temperatures. Currently, the perovskite $La_{0.6}Sr_{0.4}Co_{0.2}Fe_{0.8}O_{3-x}$ (LSCF) serves as one of the most promising cathode materials because of its high electrical and ionic conductivity at an intermediate temperature of ~750 °C [1]. Unfortunately, LSCF based cathodes have been found to experience substantial long-term degradation [2,3] which is frequently associated with Sr enrichment at the LSCF surface. The insulating nature of segregated Sr species blocks the oxygen reduction reaction (ORR) active sites or passivates the entire surface of the cathode. The Sr surface segregation is also accompanied by a reduction in transition metal concentration in the perovskite phase, causing the deterioration and decomposition of the LSCF backbone [4–9]. Surface modification through solution infiltration has been extensively investigated to enhance cathode surface functionality while retaining the advantageous qualities of the cathode backbone [10–12]. However, the effect of the infiltration largely depends on the microstructure of the infiltrate and its interaction with the backbone. The solution infiltration often ends up with discrete particles and uncontrolled distribution of infiltrated materials. Accordingly, the impact of infiltration of discrete catalyst to suppress the Sr surface segregation is limited. In addition to the solid-state phase segregation, Sr surface segregation also leads to volatile Sr species [13,14] such as SrO, $Sr(OH)_2$, $SrCO_3$, and their further interaction with volatile Cr evaporated from the interconnects of SOFC stacks [15]. To effectively mitigate the LSCF degradation associated with the Sr surface segregation, the surface coating layer on LSCF should be conformal over the entire internal surface of the cathode.

* Corresponding author.
E-mail address: xueyan.song@mail.wvu.edu (X. Song).

https://doi.org/10.1016/j.jpowsour.2021.229854
Received 22 December 2020; Received in revised form 8 March 2021; Accepted 26 March 2021
0378-7753/

Because the LSCF surface provides the electrocatalytic active site for the ORR at elevated temperatures, the protective conformal coating layer needs to be both Sr-inert and electrocatalytic. Among the electrocatalyst, Pt [16] and CoO_x [17] could be the appropriate candidates for forming a conformal coating layer. Catalytic Pt is immiscible with SrO with limited cation exchange with all elements in LSCF and provides a block of the Sr outward diffusion. On the other hand, CoO_x may have cation exchange with Fe from LSCF. CoO_x has limited diffusion of La or Sr at operating temperatures. Therefore, a CoO_x topping layer could also block the Sr cation outward diffusion. However, the catalytic activity of CoO_x on different cathode backbone remains controversial. CoO_x has been reported as an effective ORR catalyst for LSM [18]. However, for the thin film $La_{0.6}Sr_{0.4}CoO_{3-\delta}$, performance degradation was even observed upon coating CoO_x by atomic layer deposition (ALD) [19,20] and its catalytic impact on LSCF is not clear. Regardless of the catalytic activity, the as-deposited conformal coating applied to the backbone surface could interact with the backbone materials, resulting in the subsequent structure evolution and losing the conformity on the backbone surfaces at elevated temperatures.

Furthermore, once a coating layer is managed to be stabilized to be conformal on the backbone surface, it will inevitably shift the ORR pathways and potentially introduce additional electrical or ionic pathways that affect the conductivity. Here we studied the ALD [21,22] coatings of conformal Pt or CoO_x layer, respectively, onto the internal surface of LSCF/SDC cathode of inherent functional cells, and explored the possibility of forming an appropriate conformal coating layer and its resultant reaction pathway changes on the backbone surface. Upon the electrochemical operation, the ALD coated cell has resulted in the reduction of both the ohmic resistance (R_s) and polarization resistance (R_p). The electrochemical and nanostructure origin of the SOFC performance enhancement was systematically investigated using the combination of electrochemical impedance spectroscopy, the corresponding impedance spectra deconvolution, and post-operation nanostructure imaging and chemistry study.

2. Experimental section

Commercially available, anode-supported solid oxide button cells fabricated by Materials and Systems Research, Inc. (MSRI, Salt Lake City, UT) were employed for all the experiments described in this paper. MSRI cells are composed of five layers as follows, starting from the anode: a ~700 μm thick Ni/YSZ cermet layer which supports the cell structure; a ~10 μm thick Ni/YSZ active layer; a ~10 μm thick YSZ electrolyte; a thin (2–3 μm), dense Sm_2O_3-doped CeO_2 (SDC) barrier layer, a ~10 μm thick LSCF/SDC active layer; and a 50 μm thick, pure LSCF current collecting layer. The cell active area (limited by the cathode) is 2 cm^2. The exposure area of the anode to fuel is about 3.5 cm [2].

The ALD coatings were performed in a commercial GEMStar-8 ALD reactor (Arradiance Inc). The precursors used in this study were all purchased from Strem Chemicals, Inc. The (trimethyl)methylcyclopentadienylplatinum(IV), (99%) and the deionized water were used as Pt precursor and oxidant for depositing Pt layer; and the bis(cyclopentadienyl)cobalt (II), (min. 98% cobaltocene) and ozone were used as Co and oxidant, respectively, for CoO_x layer growth. During the deposition, the (trimethyl)methylcyclopentadienylplatinum and bis(cyclopentadienyl)cobalt containers were maintained at 75 °C and 90 °C, respectively; and the reactor chamber was set at 300 °C. Total 90 cycles were performed for each element deposition, leading to an ALD coating of ~7 nm Pt, or 7 nm of CoO_x, respectively. No masking or specific treatment is applied on the NiO/YSZ anode of the as-received cells before ALD processing. In practice, the thick and very dense NiO/YSZ anode prevents precursor penetration during the ALD processing, and the impact of ALD coating on the Ni/YSZ anode is negligible. No surface pretreatment was applied to the cells, and no heat-treatment was applied before or after the ALD coating either. The cell electrochemical operation was carried out directly after the ALD coating.

Three cells, including one baseline cell (cell no. 1), one with the ALD coating of Pt (cell no. 2), and one with the ALD coating of CoO_x (cell no. 3), were examined. All cell tests were performed on a test stand. The platinum mesh was used for anode and cathode lead connections. The fuel and air stream flow rates were controlled separately using mass flow controllers. Cell testing was performed at 750 °C. During the operation, a 400 mL/min air flow rate and a 400 mL/min fuel flow rate were used. Before any electrochemical measurements, both cells were current-treated for approximately ~15 h under a small current density of 0.1 A/cm^2 to ensure they were activated. The samples were loaded at a constant current of 0.3 A/cm^2 for 24 h, and then the cyclic voltammetry and impedance data were collected. The cell performance was examined using a TrueData-Load Modular Electronic DC Load, which guarantees voltage and current accuracies of 0.03% FS of the range selected ± 0.05% of the value. The cell impedance spectra were examined using a potentiostat/galvanostat (Solartron 1287A) equipped with a frequency response analyzer (Solartron 1260). Impedance measurements were carried out using a Solatron 1260 frequency response analyzer in a frequency range from 50 mHz to 100 KHz. The impedance spectra and resistances (R_s and R_p) presented are those measured under a DC bias current of 0.3 A/cm^2. On a Nyquist plot, R_s is determined by the intercept at the higher frequency end, and R_p is determined by the distance between two intercepts.

After the electrochemical operation, the ALD coated cells were sectioned and subjected to nanostructural and crystallographic examination using high resolution (HR) Transmission Electron Microscopy (TEM). On the cathode, due to the ALD coating is indifferent to substrate shape and substrate crystal orientation, both the cathode current collecting layer and the cathode active layer, the ALD coating layer is presumably covering both the LSCF current collecting layer and the LSCF/SDC active layer, that is presenting the interaction of ALD layer with both the LSCF and SDC grains. All the TEM examinations were conducted in the cathode active layer. TEM samples were prepared by mechanical polishing and ion milling in a liquid-nitrogen-cooled holder. Electron diffraction, diffraction contrast, and HRTEM imaging were performed using a JEM-2100 operated at 200 kV. Chemical analysis was carried out under TEM using energy dispersive X-ray Spectroscopy (EDS).

3. Results and discussion

3.1. Increased conductivity and shifted ORR pathway introduced by ALD coating of Pt

As shown in Fig. 1, upon the electrochemical operation at 750 °C for 24 h, the baseline cell no. 1 possesses a peak power density of 0.949 W/cm^2, with R_s of 0.111 Ω cm^2 and R_p of 0.238 Ω cm [2]. By contrast, at 24 h operation, cell no. 2 with ALD coating of Pt on the cathode backbone shows the immediate higher peak power density of 1.286 W/cm^2, which is 36% enhancement in comparison to that of the baseline.

The power density increase is accompanied by the simultaneous reduction of R_s to 0.080 Ω cm^2 by 28%, and R_p to 0.217 Ω cm^2 by 8.8%, as shown in Table 1. The enhanced conductivity in the electrode can be seen by the decrease in R_s in the Nyquist plot. To identify the physical origin of polarization resistance changes, we retrieved the dynamic constant in the impedance data by evaluating the relaxation times and relaxation amplitude of the impedance-related processes using deconvolution [23–26] (shown in Fig. 1d). The cells exhibit two arcs P1 and P2, with the frequency ranging at 2–4 Hz and 20–40 Hz, respectively, and the P1 is dominating. The P1 of ALD coated cell shifts to the higher frequency end compared to that of the baseline. In general, the physical processes occurring at the characteristic frequencies of 1–150 Hz range

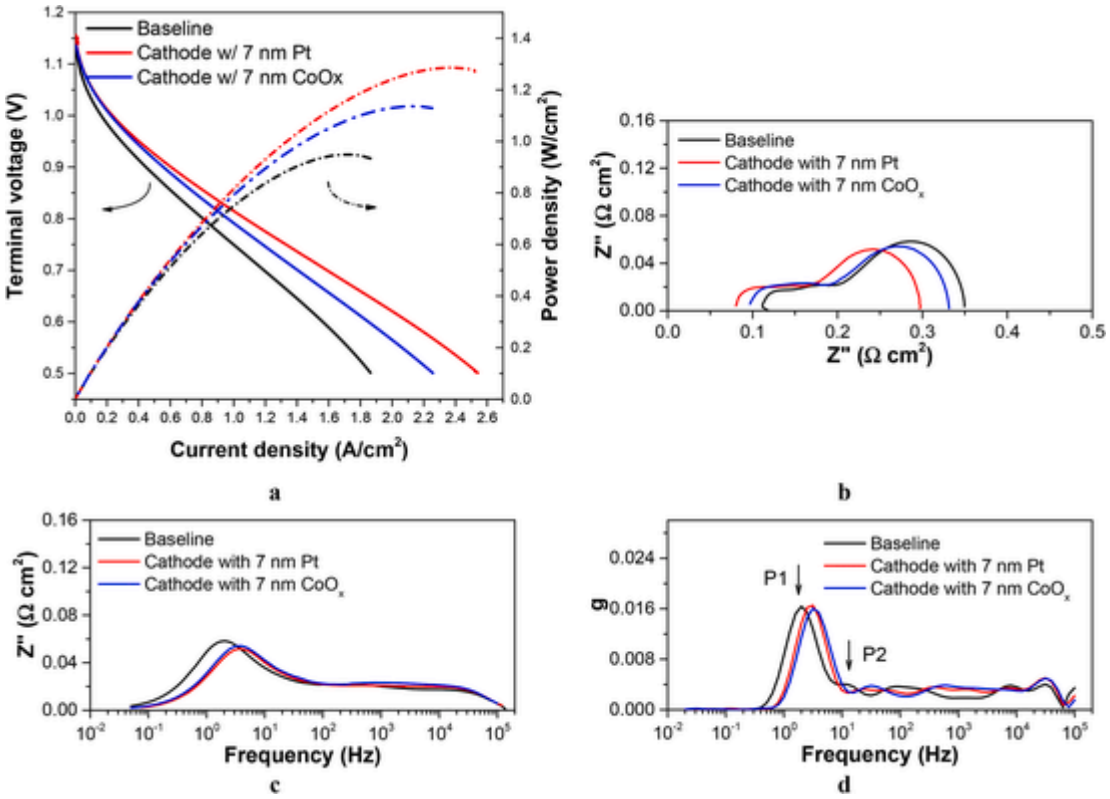

Fig. 1. Power density and impedance plots for the baseline cell no. 1, cell no. 2 LSCF cathode backbone with 7 nm Pt layer, and cell no. 3 LSCF cathode backbone with 7 nm CoO_x layer. **a** Terminal voltage as a function of current density for the cells at 750 °C. **b** Nyquist plots of four cells at a constant current of 0.3 A/cm^2. **c** Bode plots of cells at a constant current density of 0.3 A/cm^2. **d** Corresponding deconvolution spectra of the impedance data collected from two cells. Two major arcs with the frequency ranging at 2–4 Hz and 20–40 Hz are indicated by P1 and P2, respectively.

Table 1
Impedance and peak power density of the baseline cell no. 1, cell no. 2 with 7 nm Pt layer, and cell no. 3 with 7 nm CoO_x.

Cell no.	Operating time h	Cathode architecture	R_s Ω cm^2	R_p Ω cm^2	Peak Power density W/cm^2
1	24	Baseline	0.111	0.238	0.949
2	24	With 7 nm Pt	0.080	0.217	1.286
3	24	With 7 nm CoO_x	0.094	0.238	1.136

could be assigned to cathode activation polarization resistance during the ORR. Depending on the cell backbone chemistry, the peaks could shift slightly to either direction under identical cell operation conditions [27]. Since the baseline and ALD coated cells possess similar anode structures and operated under identical conditions, the slightly decreased P1 arc at 2–4 Hz is attributable to a decrease of gas diffusion and higher ORR resistance in the cathode.

The increased conductivity and change in the polarization resistance reveals that the ORR kinetics have been significantly altered in cell no. 2. The ORR and oxygen ion transport kinetics are largely affected by the nanostructure and chemistry of active electrode surfaces where the electrochemical reactions are taking place. The nanostructure and chemistry of the ALD coated cell no. 2 are thus subjected to the TEM imaging and analysis.

As shown in Fig. 2, Pt remains ~7 nm thick conformal coating layer after cell operation and covers the entire LSCF phase. Pt presents the indifferent deposition between the LSCF grains and grain boundaries. The Pt layer keeps well-defined atomic-scale binding with the LSCF grains. Moreover, there is a well-defined crystal orientation relationship between the LSCF and Pt phases in the local interface region, as shown in the Fourier Transformation. Therefore, due to the large lattice parameter difference, the interface from the well-epitaxial film is highly strained.

At the LSCF/SDC surface interfaces, the conformal coating layer extends to the SDC grains for ~100 nm. Pt phase becomes discrete further away from the LSCF/SDC surface interface. And the Pt discrete particles grew to ~70 nm in size on the SDC surface grain boundaries. According to the nanostructure analysis, the distribution of Pt in cell no. 2 is schematized in Fig. 3.

There is no cation exchange between Pt and LSCF/SDC backbone. However, the bimodal nanostructure distribution of Pt indicates that the as-deposited conformal Pt layer must have undergone a self reassembly procedure and developed strong interaction with LSCF/SDC backbone during the electrochemical reactions. According to the Pt-O_x phase diagram, the as-deposited ALD nano Pt could be vaporized as Pt–O gas species in the air at elevated temperatures. However, Pt-O_x is readily reduced during the ORR and re-assembled preferentially at the electrochemically active sites, where the oxygen partial pressure is the lowest on the cathode internal surface [28–31]. In an LSCF/SDC cathode, the oxygen adsorption and dissociation reactions take place on the LSCF surface. Subsequently, reduced oxide ions transport to the vicinity of the ionic conductor through either surface or bulk diffusion pathways. This creates a reduced atmosphere on the LSCF local surface upon the electrochemical reactions. Therefore, once the Pt is coated on LSCF, Pt remains as a dense conformal layer on the LSCF grain surfaces.

As shown in Fig. 3d, the LSCF phase and Pt phase formed an atomic bonding interface. The LSCF backbone surface seems to lose its activity for the ORR since it is entirely covered by the dense conformal Pt layer. Correspondingly, the cathode ORR sites and the related mass and charge transfer are entirely altered. The oxygen adsorption, dissociation, and the ORR take place on the Pt surfaces instead. When the Pt surface is enriched with negative oxygen ions, the dissociated oxygen

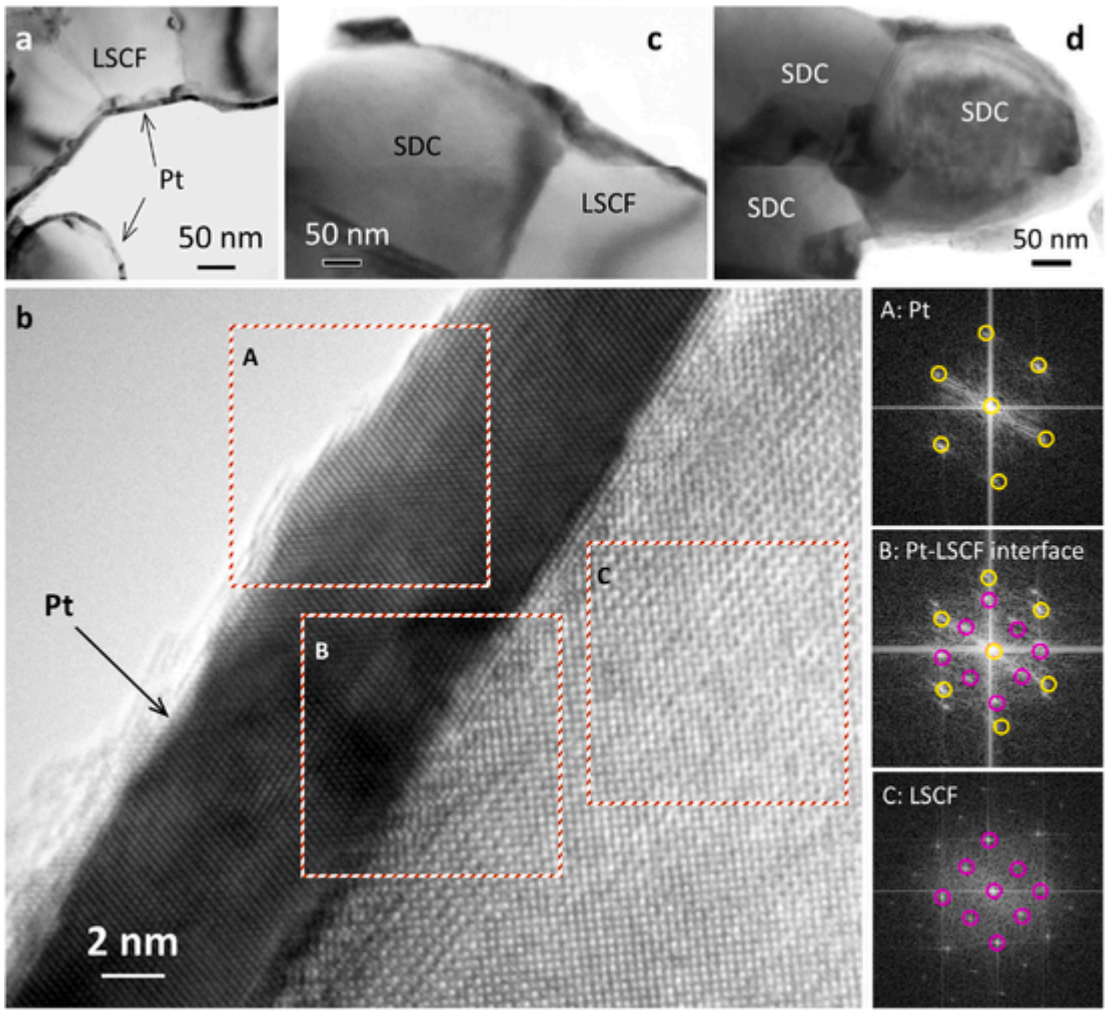

Fig. 2. TEM examination of the operated cell no. 2 with 7 nm Pt coating. **a** Conformal fully dense Pt film covering the LSCF backbone. **b** High-resolution TEM image and the related Fourier transformation showing the Pt layer is epitaxial with LSCF grain. The LSCF/Pt interface is highly strained due to the lattice mismatch. **c** Pt extended from the LSCF grain to the SDC grain surface. **d** Pt accumulated at the SDC surface grain boundaries.

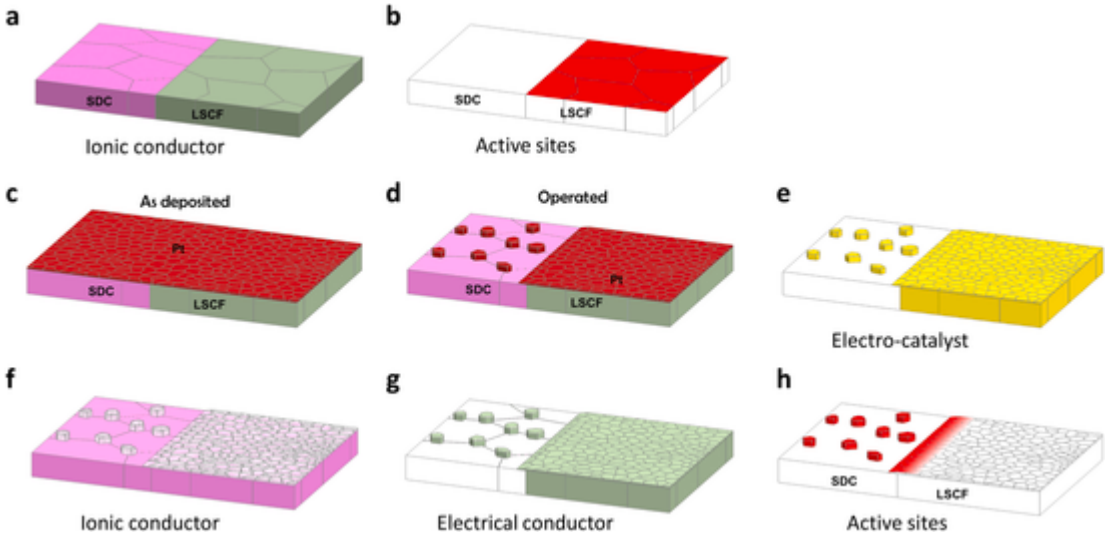

Fig. 3. Schematic of the surface architecture of the baseline cell no. 1 and cell no. 2 LSCF cathode backbone with 7 nm Pt layer. (a) Baseline LSCF phase and SDC phase and their phase boundary (interface). (b) Active ORR sites for baseline cell no. 1. (c) cell no. 2 cathode backbone with as-deposited conformal Pt layer. (d) Distribution of Pt surface layer after the electrochemical operation at 750 °C. (e) Distribution of electrocatalyst after the operation. (f) Distribution of ionic conductor after the operation. (g) Distribution of electrical conductor after the operation. (h) Expected cathode active ORR sites for cell no. 2.

ion could go through the Pt surface diffusion, through the "spillover" mechanisms, to the LSCF/SDC interface since the Pt has very low intragranular oxygen ion permeability [32]. This is consistent with Fig. 2, showing the conformal Pt layer is stable across the LSCF/SDC interface and extends ~100 nm onto the SDC surface, which is the electrochemically active region that can be extended through polarization.

Interestingly, there is an accumulation of the Pt on the SDC surface grain boundaries, as shown in Fig. 2c. In general, the SDC is an excellent ionic conductor with negligible electrical conductivity in the air. Since the Pt is deposited solely on the electrochemical reaction sites with reduced local atmosphere, the distribution of Pt grains reveals that the SDC/SDC surface grain boundaries are the active sites for the oxygen reduction reaction, and SDC/SDC surface grain boundaries are carrying the sufficient electrical conductivity. Furthermore, it is well-known that the SDC is a mixed conductor under a reducing atmosphere due to the mixed-valence state of Ce^{4+} changes to Ce^{3+} [33]. The electrical conductivity along the SDC surface grain boundaries is expected to be further enhanced due to the deposition of the Pt and subsequent further oxygen reduction reactions taking place at the SDC surface grain boundaries [34]. In other words, for the SDC surface that is originally not active for electrochemical reactions, the existence of catalytic nano-Pt on the SDC surface enabled the formation of the electrochemically active sites over the entire surface of SDC for enhanced electrochemical reactions and reduced polarization resistance.

R_s of the ALD coated cell is also decreased. At elevated temperatures, Pt shows much higher electrical conductivity (~$2.7x10^6$ S/m for Pt at 750 °C, extrapolated data) [35] and negligible ionic conductivity compared to LSCF. The reduced R_s could be attributed to the additional faster electrical pathway from the Pt layer. Meanwhile, it is worth pointing out that the Pt and LSCF have atomic-scale bonding, and the LSCF grains are significantly strained due to the large lattice mismatch between the LSCF and Pt, as shown in Fig. 3. Since the Pt is with a lattice parameter of 3.912 Å and smaller than the LSCF lattice parameter of ~3.925 Å, there is a compressive strain imposed on the LSCF grain surface. Such compressive strain would decrease the local ionic conductivity of the LSCF surface layer and offset the conductivity increased by the Pt layer [36,37]. For the LSCF/SDC coated with Pt, all reaction steps other than the transport of oxide ions in the mixed ionic and electrical conducting electrodes are facile. Once the conformal layer itself carriers higher conductivity, even if it is very thin such as ~7 nm, it would substantially lower the R_s of the cathode and, consequently, the entire cell. This is very different from the impact of discrete nanoparticles introduced by solution-based infiltration. To the best of our knowledge, all the effective solution-based infiltrations for the cathode only result in the reduction of the polarization resistance, not the series resistance. For the LSCF/SDC mixed conducting cathode backbone, our result of the conformal coating of Pt unveils that R_s of the entire cell can also be significantly reduced by applying a nano-scale thin film on the mixed conducting cathode backbone. This conclusion offers remarkable tuneability of the conductivity by further engineering the internal surface of inherent functional SOFC.

Overall, the Pt coating could have introduced two ORR pathways on the LSCF grain surfaces and SDC grain surfaces, respectively, as shown in Fig. 3. On the SDC grains, there are active sites along the SDC surface grain boundaries. On the LSCF backbone, the ORR sites are lifted from the original LSCF surfaces to the Pt surfaces. However, due to the low oxygen ion permeability in Pt and the conformality of Pt, the active sites on the LSCF backbone are limited to the LSCF/SDC interface region. Lower oxygen partial pressure of the LSCF grains could stabilize the Pt to a metallic state, ensuring the long-term stability of the LSCF without the Sr surface segregation. Because the conformal Pt coating layer does not have the Sr diffusion from the backbone either, covering the LSCF with a conformal ALD layer appears feasible to prevent the Sr surface segregation that is originally taking place on the LSCF grain surface, and such conformal ALD coating is expected to increase the cell durability over the long term.

3.2. Strained interface for accelerated ionic conductivity introduced by ALD coating of CoO_x

The different Pt interaction with LSCF than that of the SDC is presumably due to their different conductivity, especially the locally different surface properties and different local oxygen partial pressure on the grain surfaces. There are significant synergetic interactions between the ALD layer and the backbone. Such interaction is further confirmed and manifested by the ALD coating of a CoO_x layer on the cell with an identical LSCF/SDC cathode.

Cell no. 3 with a 7 nm CoO_x layer shows the immediate higher peak power density of 1.136 W/cm^2, which is a 20% enhancement compared to that of the baseline cell no. 1. The power density increase is accompanied by the reduction of R_s to 0.094 Ω cm^2 by ~18%, while the R_p of 0.238 Ω cm^2 remains unchanged to the baseline cell.

The as-deposited CoO_x layer is polycrystalline with a grain size of ~10 nm, and the layer thickness is ~7 nm over the backbone surface [38]. The CoO_x coating layer interacts strongly with the backbone upon the operation and experiences different morphology evolution depending on backbone phases. After the operation, the CoO_x layer grew into discrete nano-particles with smaller ~20 nm CoO_x grains on the LSCF surfaces (in Fig. 4 a) but much larger ~100 nm CoO_x islands on the SDC surfaces (in Fig. 4 b). Specifically, the CoO_x on the LSCF surface is high density and is close to the neighboring grains. EDS examination indicates the CoO_x grains on the LSCF surface is doped with Fe of ~2%.

The nanostructure evolution of the CoO_x layer and the resultant electrical and ionic pathway changes on the LSCF/SDC backbone are schematized in Fig. 5. The ALD coated cell remained the same polarization resistance as that of the baseline, and this is because the CoO_x possesses inferior catalytic activity than LSCF. When the discrete CoO_x is covering the LSCF grain surface, it reduces the catalytic activity of LSCF. Meanwhile, there is no solubility of Co inside the SDC grains. It has been demonstrated that a pronounced increase of the Ce^{3+} components comparing the pure CeO_2 was present in Co_3O_4/CeO_2 composite materials containing up to 30% of Co [39]. In the present study, when the CoO_x sits on the mixed conducting SDC grain boundaries, the SDC surface conductivity could be further enhanced during the oxygen reduction reactions due to the change of Ce^{4+} to Ce^{3+}. The SDC surface decorated with CoO_x becomes the active site for oxygen reduction reaction and compensates for the increase of the polarization resistance on the LSCF grain surface. Overall, the ALD coated cell depicts the comparable polarization resistance in comparison with that of the baseline.

On the other hand, R_s of the CoO_x coated cell is decreased by 18%. Such a reduction is smaller than that of cell no. 2 with Pt coating. Considering the discrete nature of the CoO_x phase on both the LSCF/SDC grains, such a reduction of R_s is impressive. On the LSCF surface, the CoO_x grains is with a minimal amount of Fe, implying cation exchange between deposited Co and Fe from LSCF may occur. For the perovskite LSCF, Co ions on the Co/Fe sites have smaller binding energy for oxygen than that with Fe ions. Increasing the Co content in LSCF could increase the electrical conductivity of the LSCF backbone [2]. Simultaneously, the deposited CoO_x layer on the SDC surface developed into the larger CoO_x grains. The discrete CoO_x grains exhibit a well-defined crystal orientation relationship with the underneath SDC phase, as shown in the Fourier Transformation in Fig. 4 c.

Due to the large lattice parameter difference [40,41], the interface from the well-epitaxial CoO_x grains and the SDC backbone is highly strained. The strained interface between the SDC and CoO_x might also provide fast ionic conducting pathways and increased electrocatalytic activity [42]. However, the CoO_x on SDC grain surface is discrete. So the effectiveness of the increased conductivity due to CoO_x coating on

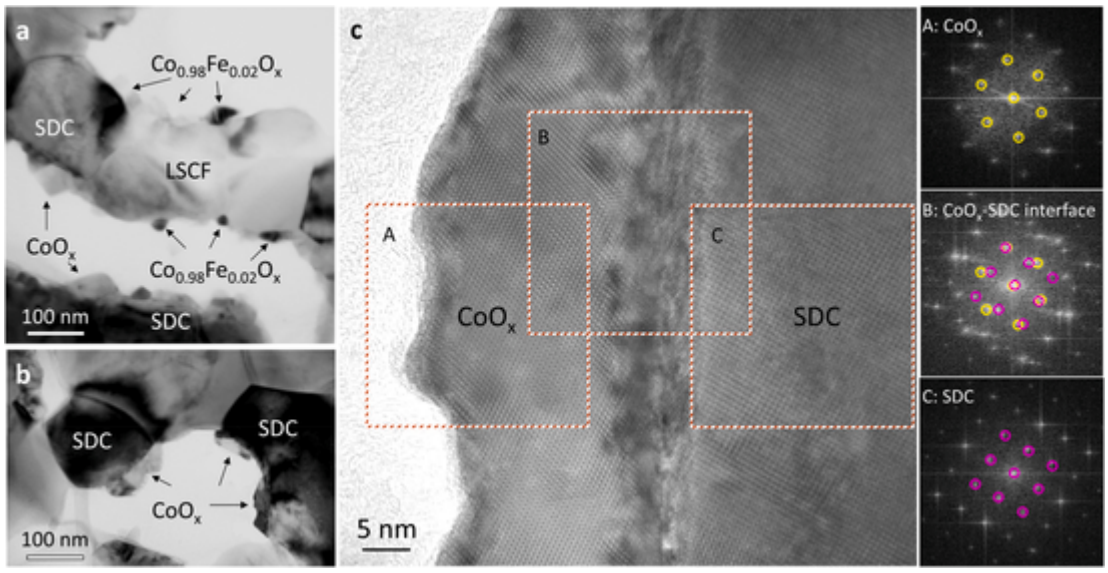

Fig. 4. TEM examination of the operated cell no. 3 with 7 nm CoO_x coating. (a) CoO_x interacts with LSCF, discrete $(Co_{0.98}Fe_{0.02})O_x$, pinned on LSCF. (b) CoO_x discrete nano-grains on the surface of mixed conductor SDC. (c) High-resolution TEM image and the related Fourier transformation show that the CoO_x layer is epitaxial with SDC grain, and the CoOx/SDC interface is highly strained due to the lattice mismatch.

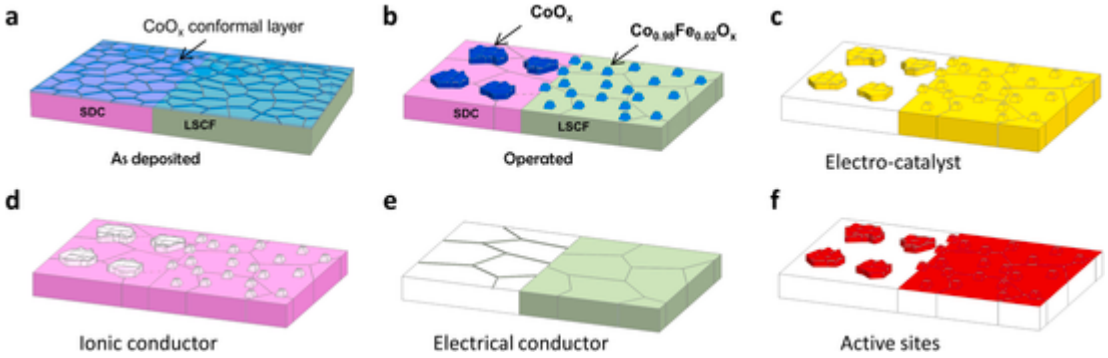

Fig. 5. Schematic of the surface architecture of cell no. 3 LSCF cathode backbone with 7 nm CoO_x layer. (a) Cell no. 3 cathode backbone with as-deposited conformal CoO_x layer. (b) Distribution of surface discrete CoO_x particles after the electrochemical operation at 750 °C. (c) Distribution of electrocatalyst after the operation. (d) Distribution of ionic conductor after the operation. (e) Distribution of electrical conductor after the operation. (f) Expected cathode active ORR sites for cell no. 3.

SDC could be much inferior to that of Pt coating. R_s is expected to be further lowered if the CoO_x can be managed to be a continuous layer.

4. Summary

There is significant interaction between the backbone phases and the ALD Pt or CoO_x layers during the electrochemical operations. Both the Pt and CoO_x surface layers went through the re-assembly during the electrode reaction. Although the Pt and CoO_x undergo completely different nanostructure evolution, they share the same feature of a bimodal distribution on different-phase surfaces. The surface layer reassembly depends on the ALD layer chemistry, the electrochemical activity of the LSCF/SDC backbone surface, and the related local oxygen partial pressure. For the ORR taking place on the LSCF/SDC electrode surface, it is feasible to apply an electrocatalytic conformal layer to prevent cations out-diffusion and mitigate the cation surface segregation. This study also unveils that the series resistance of the entire cell can be reduced by applying a nano-scale thin film on the mixed conducting cathode backbone. This offers remarkable tuneability of the conductivity by further engineering the architecture from the internal surface of a porous electrode.

CRediT authorship contribution statement

Yun Chen: Conceptualization, Methodology, Investigation, Formal analysis, Data curation, Writing – original draft, Writing – review & editing. **Sergio A. Paredes-Navia:** Investigation, Formal analysis, Data curation. **Cesar-Octavio Romo-De-La-Cruz:** Investigation, Methodology, Investigation, Writing – review & editing. **Liang Liang:** Methodology, Investigation. **Andre Fernandes:** Writing – review & editing. **Alec Hinerman:** Investigation, Formal analysis, Data curation. **Jacky Prucz:** Conceptualization, Writing – review & editing, Supervision. **Mark Williams:** Conceptualization, Formal analysis, Writing – review & editing. **Xueyan Song:** Conceptualization, Methodology, Investigation, Formal analysis, Writing – original draft, Writing – review & editing, Data curation, Supervision, Project administration, Funding acquisition.

Declaration of competing interest

The authors declare that they have no known competing financial interests or personal relationships that could have appeared to influence the work reported in this paper.

Acknowledgment

X. S., S. P., C. R., A. H., L. L., Y. C. acknowledge the financial support from DE-FE0031665, DE-FE 0031251, DE-FE0026167. X. S acknowledges the support from NSF-DMR 1916581.

References

[1] S.P. Jiang, Development of lanthanum strontium cobalt ferrite perovskite electrodes of solid oxide fuel cells – a review, Int. J. Hydrogen Energy 44 (14) (2019) 7448–7493.
[2] P. Hjalmarsson, M. Søgaard, M. Mogensen, Electrochemical performance and degradation of $(La_{0.6}Sr_{0.4})_{0.99}CoO_{3-\delta}$ as porous SOFC-cathode, Solid State Ionics 179 (27) (2008) 1422–1426.
[3] S.P. Simner, M.D. Anderson, M.H. Engelhard, J.W. Stevenson, Degradation mechanisms of La–Sr–Co–Fe–O_3 SOFC cathodes, Electrochem. Solid State Lett. 9 (10) (2006) A478.
[4] H. Okamoto, G. Kawamura, T. Kudo, Study of oxygen adsorption on platinum through observation of exchange current in a solid electrolyte concentration cell, Electrochim. Acta 28 (3) (1983) 379–382.
[5] H. Hu, M. Liu, Interfacial polarization characteristics of Pt | $BaCe_{0.8}Gd_{0.2}O_3$ | Pt cells at intermediate temperatures, J. Electrochem. Soc. 144 (10) (1997) 3561–3567.
[6] E. Schouler, G. Giroud, M. Kleitz, Applications selon Bauerle du tracé des diagrammes d'admittance complexe en électrochimie des solides, J. Chim. Phys. 70 (1973) 1309–1316.
[7] M.J. Verkerk, M.W.J. Hammink, A.J. Burggraaf, Oxygen transfer on substituted ZrO_2, Bi_2O_3, and CeO_2 electrolytes with platinum electrodes: I. Electrode resistance by D-C polarization, J. Electrochem. Soc. 130 (1) (1983) 70–78.
[8] R. Lewis, R. Gomer, Adsorption of oxygen on platinum, Surf. Sci. 12 (2) (1968) 157–176.
[9] J. Mizusaki, K. Amano, S. Yamauchi, K. Fueki, Electrode reaction at Pt, O_2(g)/stabilized zirconia interfaces. Part I: theoretical consideration of reaction model, Solid State Ionics 22 (1987) 313–322.
[10] R. Tomov, T. Mitchel-Williams, R. Maher, G. Kerherve, L. Cohen, D. Payne, R. Kumar, B. Glowacki, The synergistic effect of cobalt oxide and Gd-CeO_2 dual infiltration in LSCF/CGO cathodes, J. Mater. Chem. 6 (2018) 5071–5081.
[11] N. Ai, S. He, N. Li, Q. Zhang, W.D. Rickard, K. Chen, T. Zhang, S.P. Jiang, Suppressed Sr segregation and performance of directly assembled $La_{0.6}Sr_{0.4}Co_{0.2}Fe_{0.8}O_{3-\delta}$ oxygen electrode on Y_2O_3-ZrO_2 electrolyte of solid oxide electrolysis cells, J. Power Sources 384 (2018) 125–135.
[12] H. Ding, A.V. Virkar, M. Liu, F. Liu, Suppression of Sr surface segregation in $La_{1-x}Sr_xCo_{1-y}Fe_yO_{3-\delta}$: a first principles study, Phys. Chem. Chem. Phys. 15 (2013) 489–496.
[13] F. Tietz, A. Mai, D. Stöver, From powder properties to fuel cell performance – a holistic approach for SOFC cathode development, Solid State Ionics 179 (2008) 1509–1515.
[14] H. Yokokawa, H. Tu, B. Iwanschitz, A. Mai, Fundamental mechanisms limiting solid oxide fuel cell durability, J. Power Sources 182 (2008) 400–412.
[15] Z. Yang, G.-G. Xia, X.-H. Li, J.W. Stevenson, $(Mn,Co)_3O_4$ spinel coatings on ferritic stainless steels for SOFC interconnect applications, Int. J. Hydrogen Energy 32 (2007) 3648–3654.
[16] I.E. Stephens, A.S. Bondarenko, U. Grønbjerg, J. Rossmeisl, I. Chorkendorff, Understanding the electrocatalysis of oxygen reduction on platinum and its alloys, Energy Environ. Sci. 5 (2012) 6744–6762.
[17] D. Chen, C. Huang, R. Ran, H.J. Park, C. Kwak, Z. Shao, New $Ba_{0.5}Sr_{0.5}Co_{0.8}Fe_{0.2}O_{3-\delta} + Co_3O_4$ composite electrode for IT-SOFCs with improved electrical conductivity and catalytic activity, Electrochem. Commun. 13 (2011) 197–199.
[18] K. Yamahara, C.P. Jacobson, S.J. Visco, X.F. Zhang, L.C. de Jonghe, Thin film SOFCs with cobalt-infiltrated cathodes, Solid State Ionics 176 (2005) 275–279.
[19] E. Mutoro, E.J. Crumlin, M.D. Biegalski, H.M. Christen, Y. Shao-Horn, Enhanced oxygen reduction activity on surface-decorated perovskite thin films for solid oxide fuel cells, Energy Environ. Sci. 4 (2011) 3689–3696.
[20] H.J. Choi, K. Bae, D.Y. Jang, J.W. Kim, J.H. Shim, Performance degradation of lanthanum strontium cobaltite after surface modification, J. Electrochem. Soc. 162 (2015) F622–F626.
[21] B.J. O'Neill, D.H. Jackson, J. Lee, C. Canlas, P.C. Stair, C.L. Marshall, J.W. Elam, T.F. Kuech, J.A. Dumesic, G.W. Huber, Catalyst design with atomic layer deposition, ACS Catal. 5 (2015) 1804–1825.
[22] T. Onn, R. Küngas, P. Fornasiero, K. Huang, R. Gorte, Atomic layer deposition on porous materials: problems with conventional approaches to catalyst and fuel cell electrode preparation, Inorganics 6 (2018) 34.
[23] V. Sonn, A. Leonide, E. Ivers-Tiffée, Combined deconvolution and CNLS fitting approach applied on the impedance response of technical Ni/8YSZ cermet electrodes, J. Electrochem. Soc. 155 (2008) B675–B679.
[24] B. Liu, H. Muroyama, T. Matsui, K. Tomida, T. Kabata, K. Eguchi, Analysis of impedance spectra for segmented-in-series tubular solid oxide fuel cells, J. Electrochem. Soc. 157 (2010) B1858–B1864.
[25] R. Barfod, M. Mogensen, T. Klemenso, A. Hagen, Y.-L. Liu, P. Vang Hendriksen, Detailed characterization of anode-supported SOFCs by impedance spectroscopy, J. Electrochem. Soc. 154 (2007) 371–378.
[26] A. Leonide, B. Ruger, A. Weber, W.A. Meulenberg, E. Ivers-Tiffee, Impedance study of alternative $(La,Sr)FeO_{3-\delta}$ and $(La,Sr)(Co,Fe)O_{3-\delta}$ MIEC cathode compositions, J. Electrochem. Soc. 157 (2010) B234–B239.
[27] M. Kornely, A. Neumann, N.H. Menzler, A. Leonide, A. Weber, E. Ivers-Tiffee, Degradation of anode supported cell (ASC) performance by Cr-poisoning, J. Power Sources 196 (2011) 7203–7208.
[28] S.M. Shin, B.Y. Yoon, J.H. Kim, J.M. Bae, Performance improvement by metal deposition at the cathode active site in solid oxide fuel cells, Int. J. Hydrogen Energy 38 (2013) 8954–8964.
[29] Y. Xiong, K. Yamaji, H. Kishimoto, M.E. Brito, T. Horita, H. Yokokawa, Deposition of platinum particles at LSM/ScSZ/Air three-phase boundaries using a platinum current collector, Electrochem. Solid State Lett. 12 (2009) B31–B33.
[30] Y. Chen, K. Gerdes, S. Paredes Navia, L. Liang, A. Hinerman, X. Song, Conformal electrocatalytic surface nanoionics for accelerating high-temperature electrochemical reactions in solid oxide fuel cells, Nano Lett. 19 (12) (2019) 8767–8773.
[31] Y. Chen, L. Liang, S. Paredes Navia, A. Hinerman, K. Gerdes, X. Song, Synergetic interaction of additive dual nanocatalysts to accelerate oxygen reduction reaction in fuel cell cathodes, ACS Catal. 9 (8) (2019) 6664–6671.
[32] F.K. Moghadam, D.A. Stevenson, Oxygen diffusion and solubility studies in Ag and Pt using AC impedance spectroscopy, J. Electrochem. Soc. 133 (1986) 1329–1332.
[33] X.D. Zhou, W. Huebner, I. Kosacki, H.U. Anderson, Microstructure and grain-boundary effect on electrical properties of gadolinium-doped ceria, J. Am. Ceram. Soc. 85 (2002) 1757–1762.
[34] A. Nenning, A. Opitz, Low oxygen partial pressure increases grain boundary ion conductivity in Gd-doped ceria thin films, J. Phys.: Energy 2 (2019) 014002.
[35] R.W. Powell, R. Tye, M.J. Woodman, Thermal conductivities and electrical resistivities of the platinum metals, Platin. Met. Rev. 6 (4) (1962) 138–143.
[36] S. Lee, J.L. MacManus-Driscoll, Research Update: fast and tunable nanoionics in vertically aligned nanostructured films, Apl. Mater. 5 (2017) 042304.
[37] J.L. MacManus-Driscoll, P. Zerrer, H. Wang, H. Yang, J. Yoon, A. Fouchet, R. Yu, M. G. Blamire, Q. Jia, Strain control and spontaneous phase ordering in vertical nanocomposite heteroepitaxial thin films, Nat. Mater. 7 (2008) 314–320.
[38] Y. Chen, A. Hinerman, L. Liang, K. Gerdes, S.P. Navia, J. Prucz, X. Song, Conformal coating of cobalt oxide on solid oxide fuel cell cathode and resultant continuously increased oxygen reduction reaction kinetics upon operation, J. Power Sources 405 (2018) 45–50.
[39] L. Liotta, G. Di Carlo, G. Pantaleo, A. Venezia, G. Deganello, Co_3O_4/CeO_2 composite oxides for methane emissions abatement: relationship between Co_3O_4–CeO_2 interaction and catalytic activity, Appl. Catal. B Environ. 66 (2006) 217–227.
[40] A. Steel, E. McIntyre, J. Harnett, H. Foley, J. Adams, D. Sibbritt, J. Wardle, J. Frawley, Complementary medicine use in the Australian population: results of a nationally-representative cross-sectional survey, Sci. Rep. 8 (2018) 1–7.
[41] H. Okkay, M. Bayramoglu, M.F. Öksüzömer, $Ce_{0.8}Sm_{0.2}O_{1.9}$ synthesis for solid oxide fuel cell electrolyte by ultrasound assisted co-precipitation method, Ultrason. Sonochem. 20 (2013) 978–983.
[42] J.R. Petrie, C. Mitra, H. Jeen, W.S. Choi, T.L. Meyer, F.A. Reboredo, J.W. Freeland, G. Eres, H.N. Lee, Strain control of oxygen vacancies in epitaxial strontium cobaltite films, Adv. Funct. Mater. 26 (2016) 1564–1570.